

Primary Neural Degeneration in the Human Cochlea: Evidence for Hidden Hearing Loss in the Aging Ear

P. Z. Wu,^{a,b,c} L. D. Liberman,^a K. Bennett,^d V. de Gruttola,^d J. T. O'Malley^a and M. C. Liberman^{a,b*}

^a Eaton-Peabody Laboratories, Massachusetts Eye and Ear, Boston, MA 02114, USA

^b Department of Otolaryngology, Harvard Medical School, Boston, MA 02115, USA

^c Department of Otorhinolaryngology Head and Neck Surgery, The First Affiliated Hospital, Sun Yat-sen University, Guangzhou 510080, China

^d Department of Biostatistics, Harvard TH Chan School of Public Health, Boston, MA 02115, USA

Abstract—The noise-induced and age-related loss of synaptic connections between auditory-nerve fibers and cochlear hair cells is well-established from histopathology in several mammalian species; however, its prevalence in humans, as inferred from electrophysiological measures, remains controversial. Here we look for cochlear neuropathy in a temporal-bone study of “normal-aging” humans, using autopsy material from 20 subjects aged 0–89 yrs, with no history of otologic disease. Cochleas were immunostained to allow accurate quantification of surviving hair cells in the organ Corti and peripheral axons of auditory-nerve fibers. Mean loss of outer hair cells was 30–40% throughout the audiometric frequency range (0.25–8.0 kHz) in subjects over 60 yrs, with even greater losses at both apical (low-frequency) and basal (high-frequency) ends. In contrast, mean inner hair cell loss across audiometric frequencies was rarely >15%, at any age. Neural loss greatly exceeded inner hair cell loss, with 7/11 subjects over 60 yrs showing >60% loss of peripheral axons *re* the youngest subjects, and with the age-related slope of axonal loss outstripping the age-related loss of inner hair cells by almost 3:1. The results suggest that a large number of auditory neurons in the aging ear are disconnected from their hair cell targets. This primary neural degeneration would not affect the audiogram, but likely contributes to age-related hearing impairment, especially in noisy environments. Thus, therapies designed to regrow peripheral axons could provide clinically meaningful improvement in the aged ear.

This article is part of a Special Issue entitled: Hearing Loss, Tinnitus, Hyperacusis, Central Gain. © 2018 The Author(s). Published by Elsevier Ltd on behalf of IBRO. This is an open access article under the CC BY-NC-ND license (<http://creativecommons.org/licenses/by-nc-nd/4.0/>).

Key words: hidden hearing loss, cochlear neuropathy, human temporal bone, aging.

INTRODUCTION

Although sensorineural hearing loss (SNHL) can involve damage to either sensory cells or sensory neurons of the inner ear, a longstanding dogma in acquired SNHL was that loss of sensory cells is the primary event, and that degeneration of auditory nerve fibers (ANFs) occurs only secondarily to the loss of peripheral targets (Bohne and Harding, 2000). If ANFs were lost only after hair cells die, then neural degeneration would contribute little to hearing deficit in acquired SNHL except in the context of a cochlear implant.

This view arose because, after cochlear insults such as acoustic injury or ototoxic drugs, the degeneration of

sensory cells can be seen within hours post-exposure, whereas degeneration of spiral ganglion cells (SGCs), the cell bodies of the ANFs, is not visible for weeks to months (Liberman and Kiang, 1978). Animal work challenged the dogma by showing that hair cell loss in acquired SNHL is neither necessary nor sufficient for loss of ANFs. Firstly, in acoustic injury models, overexposures causing only reversible threshold shifts, and no hair cell loss, can nevertheless cause significant ANF degeneration (Kujawa and Liberman, 2009; Furman et al., 2013). The neural damage is visible immediately as loss of synaptic connections between ANFs and inner hair cells (IHCs), while loss of ANF peripheral axons is not obvious for several weeks, and loss of SGCs and central axons progresses for months to years (Johnsson, 1974; Johnsson and Hawkins, 1976; Kujawa and Liberman, 2009). In the aging mouse ear, as in the noise-damaged ear, it is the connections between SGCs and IHCs that degenerate first, rather than the hair cells themselves (Stamatakis et al., 2006; Sergeyenko et al., 2013). This primary neural degeneration, or partial de-afferentation of IHCs, has negligible

*Correspondence to: M.C. Liberman, Eaton-Peabody Laboratories, Massachusetts Eye and Ear Infirmary, 243 Charles St., Boston, MA 02114-3096, USA.

E-mail address: Charles.Liberman@meei.harvard.edu (M. C. Liberman).
Abbreviations: ANFs, auditory nerve fibers; EDTA, Ethylenediaminetetraacetic acid; IHCs, inner hair cells; MEEI, Massachusetts Eye and Ear Infirmary; SGCs, spiral ganglion cells; SNHL, sensorineural hearing loss.

effect on thresholds until it exceeds 80–90% (Woellner and Schuknecht, 1955; Lobarinas et al., 2013), thus it “hides” behind the audiogram. Lastly, in transgenic mouse lines where IHCs can be destroyed by driving or blocking metabolic pathways intrinsic to the hair cells themselves, i.e. without introduction of trauma or toxins to the entire cochlear duct, hair cell loss is not sufficient to cause neural degeneration, at least for survival times out to several months (Zilberstein et al., 2012; Tong et al., 2015).

The observation that ANF degeneration precedes and/or exceeds hair cell loss in animal models of acquired SNHL has suggested why two people with the same threshold audiogram, whether normal or abnormal, can have very different abilities to understand speech in a noisy environment (Badri et al., 2011; Vermiglio et al., 2012). i.e. that partial de-afferentation of IHCs, a.k.a. “hidden hearing loss”, compromises hearing ability in complex listening environments without changing the ability to detect a pure tone in quiet. This line of thinking has inspired experiments to look in “normal-hearing” human subjects for correlations between speech-in-noise scores and various electrophysiological measures of cochlear neural health (Lieberman et al., 2016).

Here we take a direct approach to the question of whether hidden hearing loss is as important in humans as in animal models. We study temporal bones from a group of “normal-aging” humans, ranging in age from birth to 86 yrs, without any explicit history or ear diseases or ototoxic exposures. We prepare these autopsy specimens in ways that allow us to accurately quantify the survival of hair cells and ANF peripheral axons in the same cochlear regions. We show that the age-related loss of ANFs is almost three times steeper than the loss of IHCs, and thus that there is a steady, age-related increase in the degree of de-afferentation of surviving hair cells, which likely contributes significantly to the steady decline in overall hearing ability.

METHODS

Subjects and groups

The materials for the present study are human temporal bones obtained at autopsy. Based on the autopsy notes and medical histories, we selected 29 ears that have no overt otologic disease and no exposure to known ototoxic agents (except for one 24-yr old, included because autopsy material is so rare in that age range: Table 1). As summarized in Table 1, these cases range in age from birth to 86 yrs, and include 16 males and 13 females. Most of the ears (20/29) were processed as immunostained wholemounts of the sensory epithelium, where 3-D image stacks of neurons and hair cells can be obtained in the confocal microscope. Seven ears were serially sectioned celloidin-embedded cases selected from the temporal-bone archives at the Massachusetts Eye and Ear Infirmary (MEEI), and data from two ears were extracted from a publication from another group (Spoendlin and Schrott, 1990). Further details are available in Table 1. All procedures were approved by the Human Studies Committee of the Massachusetts Eye and Ear Infirmary.

Cochlear processing

Ears to be analyzed as wholemounts were extracted with a bone-plugging tool (Schuknecht, 1993) soon after death and immediately immersed in buffered 10% formalin after opening the round and oval windows. After post-fixation (4 °C) for at least 6 days, the bone plug containing the cochlea was drilled to remove as much of the petrous bone as possible, and then immersed in EDTA at room temperature for ~27 days. The cochlea was then microdissected into 8–9 pieces, each containing the osseous spiral lamina and the attached organ of Corti. Following immunostaining, the cochlear spiral was mapped by tracing an arc along the line representing the junction between inner and outer pillar heads, and normalized cochlear length was converted to frequency using a type of Greenwood function (Greenwood, 1990) modified to produce best frequencies at the very apex and base of the cochlea of 100 Hz and 20 kHz respectively. Fourteen frequency locations from 0.175 to 16 kHz were calculated, and displayed, on low-power images of the microdissected pieces, at half-octave intervals along the length of the spiral, to pinpoint the image-acquisition loci in each case.

In each ear from the MEEI archival temporal bone collection, for each of the five half-turns of the cochlear spiral (Fig. 1A), two sections were identified for immunostaining and analysis: (1) the tangential section containing the IHCs, and (2) a section 8–10 sections (i.e. 160–200 μm) closer to the modiolus for analysis of peripheral axons in the osseous spiral lamina (Fig. 1B). In practice, the latter section was typically near the edge of the limbus where Reissner’s membrane attaches. At this radial position, all peripheral axons of type-I ANFs innervating IHCs are normally myelinated, because the length of the unmyelinated terminals of ANFs is <80 μm (Lieberman, 1980). The frequency correlate of these tangent positions was determined by first making a 2D reconstruction of the cochlea spiral (Schuknecht, 1993) and then converting normalized distance into frequency using the same mapping function described above. Prior to immunostaining, the retrieved sections were delcoidinized using organic solvents as described elsewhere in more detail (O’Malley et al., 2009).

Immunostaining protocols

For wholemounts, cochlear pieces underwent a freeze/thaw step in 30% sucrose to permeabilize them, followed by 1 h at room temperature in a blocking buffer (PBS with 5% normal horse serum and 0.3–1% Triton X-100). Tissue was then incubated overnight at 37 °C with some combination of the following primary antibodies (plus 0.3–1% TritonX): (1) mouse (IgG1) anti-CtBP2 (C-terminal Binding Protein; BD Biosciences #612044) at 1:200 to quantify pre-synaptic ribbons; (2) chicken anti-neurofilament (Chemicon #AB5539) at 1:1000 to quantify nerve axons, (3) rabbit anti-Myosin VI and/or VIIa (Proteus Biosciences #25-6791 and 25-6790, respectively) at 1:100 to count hair cells and (4) goat anti-ChAT (choline acetyltransferase; Millipore #AB144P) at 1:100 to identify efferent axons from the

Table 1. Age, sex, post-mortem time, processing technique, cause of death and medical histories for each of the cases on which the present study is based

Age (yrs)	Sex	Post-mortem (hrs)	Technique	Cause of death	Other relevant medical history
0	M	5	Celloidin Sections	Meconium aspiration, pneumothorax, pneumonia	Nothing relevant
0.02	M	7	Celloidin Sections	Cardiorespiratory failure	Polysplenia syndrome. Situs inversus. Aspiration pneumonia
0.03	M	15	Celloidin Sections	Respiratory Failure	Hydrolethalus syndrome. Dandy-Walder malformation
0.16	M	?	Wholemout	No medical history	Nothing relevant
0.9	F	3	Celloidin Sections	Fetal distress from laryngo-tracheal malacia	Repeated bronchopneumonia. Demyelination of brainstem. Hydrocephalus after choroid plexus hemorrhage
4	M	1.5	Celloidin Sections	Letterer-Siwe disease	750 rads of X-ray treatment, Chlorambucil and Velban
7	F	?	Plastic Sections	No medical history	Nothing relevant
7	F	?	Plastic Sections	No medical history	Nothing relevant
13	F	11	Celloidin Sections	Craniotomy for astrocytoma	Pringle's disease – tuberous sclerosis. Epileptic seizure, controlled with carbamazepine
23	F	9	Celloidin Sections	Cardiac arrest during surgery	Juvenile onset diabetes and chronic renal failure. Rejected pancreas and renal transplants
24	M	7.5	Wholemout	Testicular choriocarcinoma	Normal audiogram in 2014, before cisplatin chemotherapy
39	F	12	Wholemout	Hepatic encephalopathy	Cirrhosis. Rejected liver transplant
52	M	9	Wholemout	Dilated cardiomyopathy	Ethanol-related cirrhosis
54	M	8	Wholemout	Acute bronchopneumonia, septic shock	Sepsis, diabetes mellitus, chronic kidney disease, hypertension, hyper-cholesterolemia
56	M	8.5	Wholemout	Metastatic renal cell carcinoma	Right nephrectomy
56	F	6	Wholemout	Recurrent grade IV glioblastoma	Glioblastoma with surgery and radiation. Atherosclerotic coronary disease. Right breast cancer
59	F	7.5	Wholemout	Stage IV pancreatic cancer	Nothing relevant
61	M	13.5	Wholemout	Upper gastrointestinal bleed in the setting of hepatic cirrhosis	Hemochromatosis, hepatic cirrhosis.
66	F	9.25	Wholemout	Fatal Arrhythmia, Myocardial Infarction	Atherosclerotic coronary artery disease
67	F	11.5	Wholemout	Brain herniation, posterior fossa bleed	Nothing relevant
67	M	12	Wholemout	Gastrointestinal perforation	Chronic pseudomembranous colitis. Left frontal lobe glioblastoma treated with Temodar and Avastin
68	M	10	Wholemout	Diffuse large B-cell lymphoma	Nothing relevant
70	F	8.75	Wholemout	Extensive myocardial infarction	Atherosclerotic coronary artery disease. Multiple coronary bypasses
75	M	17	Wholemout	Hypotensive shock following partial hepatic resection	Colon adenocarcinoma with liver metastasis – surgically removed, no residual carcinoma
76	M	13.5	Wholemout	Acute myocardial infarction	Atherosclerotic coronary artery disease. Multiple myocardial infarctions. Prostatic adenocarcinoma
78	M	10	Wholemout	Pneumonia	Coronary arterial disease
80	F	7	Wholemout	Brain herniation, hemorrhagic stroke	Contralateral schwannoma. Pancreatic adenocarcinoma with gemcitabine and 5-FU. Hypertension with Lasix
86	F	12	Wholemout	Chronic lymphatic leukemia	Atherosclerotic coronary artery disease. Alzheimer's disease, glaucoma
89	M	5.5	Wholemout	No medical history	Nothing relevant

olivocochlear bundle. Primary incubations were followed by two sequential 60-min incubations at 37 °C in species-appropriate secondary antibodies (coupled to Alexafluor dyes) with 0.3–1% TritonX. After immunostaining, all pieces from each cochlea were slide-mounted in Vectashield, coverslipped, and the coverslip was sealed with nail polish. After analysis of synaptic ribbons, hair cells and efferent terminals, the coverslips were removed and the tissue was incubated

in a fluorescent membrane dye (CellMask® Orange, Thermo Fisher #C10045) at 1:5000 with 0.3% TritonX for 5 min to label the myelin sheaths. The pieces were re-mounted and coverslipped with Vectashield. This final treatment did not disturb the pre-existing immunostains.

The de-celloidinized archival sections were immunostained differently according to elements of interest. Tangents located in the osseous spiral lamina were stained with CellMask® to show myelin sheaths,

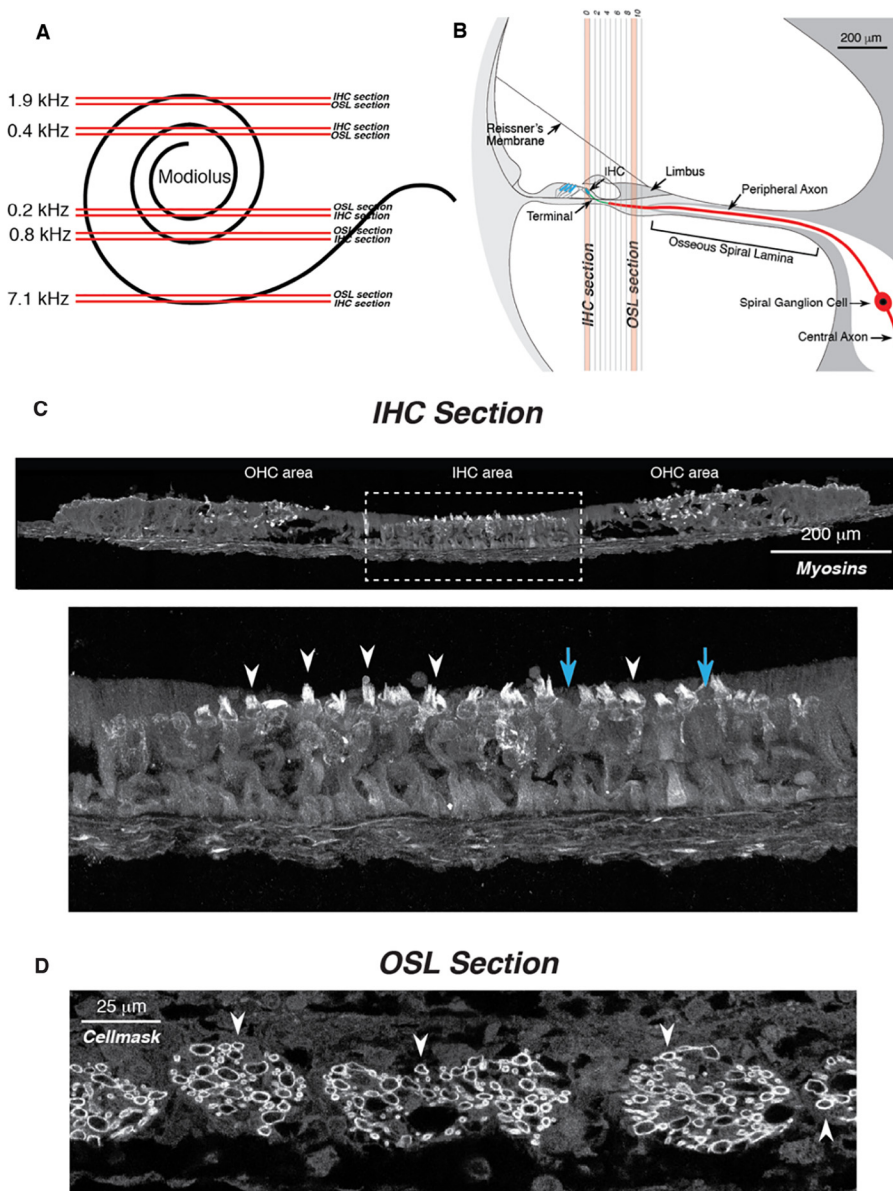


Fig. 1. The approach used to count IHCs and ANF peripheral axons in archival, sectioned human temporal bones. (A) Schematic cochlear spiral with tangential section planes indicating the pair of sections in which IHCs and ANFs were counted, and the approximate cochlear frequency regions of each. (B) Schematic cross section through the human cochlear duct showing the location of the paired tangential sections in one half turn, i.e. one through the IHCs and a second through the osseous spiral lamina, near the intersection between Reissner's membrane and the limbus. (C, D) Sample archival sections from the 0.4-kHz region of one case after de-celloidinization and staining to reveal hair cells (C) or myelinated peripheral axons (D). Inset in C (dashed box) is shown at higher magnification immediately below: white arrowheads indicate some of the IHC hair bundles immunostained with anti-myosin VIIa and anti-myosin VI. Blue arrows indicate the positions of two missing IHCs. White arrowheads in D indicate a few of the Cellmask-stained fibers in these fascicles of type I peripheral axons.

and sometimes immunostained for neurofilament and ChAT, to show afferent and efferent fibers, respectively. Tangents through the IHCs were immunostained for Myosin VI and/or VIIa. Detailed staining protocols were similar to those used for the wholemounds, as described above, except that incubations were done at room temperature.

Innervation analysis and hair cell counts

For all stained tissues, confocal z-stacks were acquired with 0.33 μm z-spacing on a Leica SP8 using a 63 \times glycerol objective (1.3 N.A.). For wholemounds, images were acquired at 14 equally spaced locations along the spiral. At each location, a region of interest, 246 \times 246 μm , encompassing the IHC region, and the adjacent osseous spiral lamina, was imaged to count peripheral axons and the number of surviving IHCs. For cytochleograms, a separate stack was acquired at each location after slight repositioning of the region of interest to include both inner and outer hair cells. For tangential sections of archival material, image stacks spanning the entire section thickness (for the IHC section) and the top 5 microns (for the osseous spiral lamina section) were separately montaged.

Hair cell fractional survival in wholemounds was quantified by counting the number of remaining cells in each row as the numerator and estimating the number of missing cells to include in the denominator. In cases with only scattered loss, missing cells are easy to count as gaps in the regular array (Fig. 2A). In cases with more massive losses (e.g. Fig. 2C), the denominator was estimated from the minimal-loss cases, using mean values as a function of cochlear location. Among the OHCs, the denominator was set by the 1st row cells, because they are always the more regularly arrayed.

Peripheral axon counts in the wholemounds were made by creating virtual slices using Amira software through the osseous spiral lamina in the xz plane, and choosing one within 100 μm of the habenula, where the CellMask®

staining was the brightest or clearest. Using that virtual section (1 voxel thick), and several on each side of it, the number of myelinated fibers was counted, using ImageJ to facilitate the counting process by placing markers on counted elements to produce a permanent data record. All fibers within the 246 μm x-span of the stack were counted, so long as they were completely

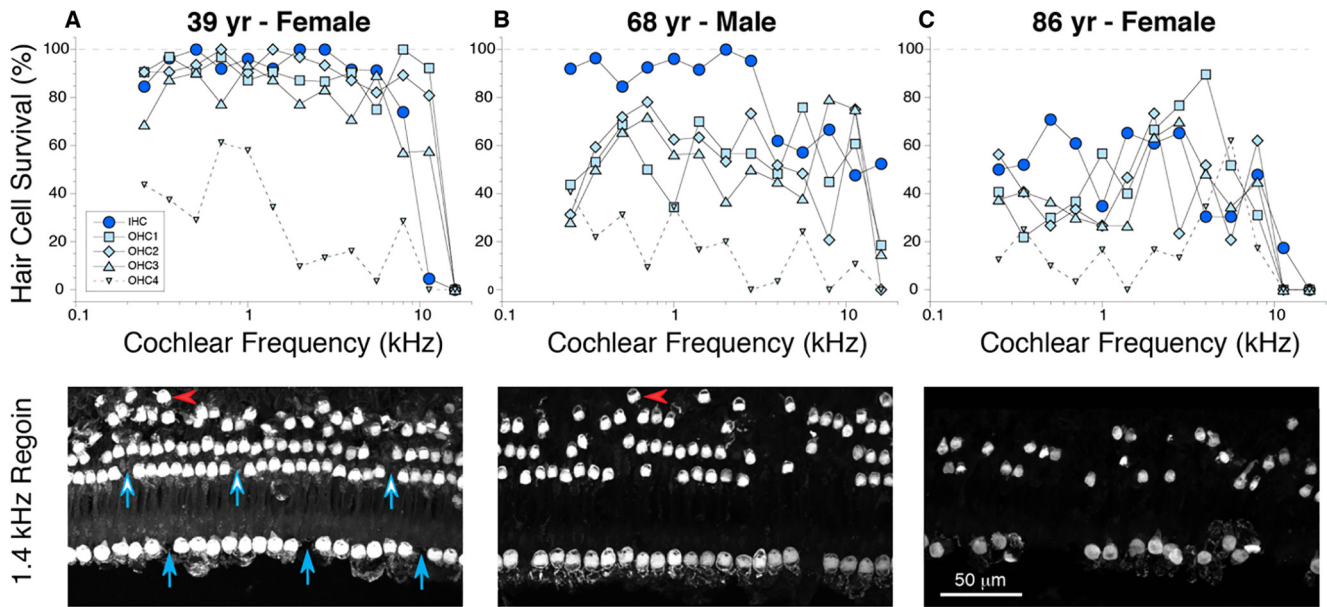


Fig. 2. Cytocochleograms from three representative specimens, paired with the respective confocal images at the 1.4-kHz region. Hair cells are visualized using antibodies to Myosin VI and/or VIIa. Arrows in A note the locations of missing IHCs (blue-filled) and 1st row OHCs (white-filled). Red arrowheads in A and B indicate two 4th row OHCs. Scale bar in C applies to all panels.

within the image, i.e. not touching the edges on either side.

Peripheral axons in de-celloidinized sections were counted by placing a 250- μm -wide rectangular region of interest over the middle of the osseous spiral lamina, precisely halfway between the two IHC regions at either end of the section, and choosing a z-plane in the selected region where the fibers were brightest. The rest of the counting process was analogous to that used for wholemount z-stacks.

The density of unmyelinated outer spiral fibers, spiraling underneath the OHCs, was quantified by averaging results from two adjacent z-stacks (each spanning 112 μm of the cochlear epithelium) at each of the 14 cochlear locations. The neurofilament channel of the z-stack maximum projection was extracted and ported to ImageJ, where the auto-thresholding algorithm was used to count the total signal in the projection, expressed as the number of suprathreshold pixels.

RESULTS

Patterns of hair cell loss

In each of the 20 wholemount cases in the present study, a cytocochleogram was constructed from confocal images sampled at 14 positions along the cochlear spiral, corresponding to half-octave intervals of frequency from 0.175 to 16 kHz (Fig. 2). Each image spanned roughly 246 μm of cochlear length, which should contain about 25 hair cells in each row. The immunostain for Myosin VI and VIIa was remarkably robust, especially in the hair cell cuticular plates, thus the hair cell counts were quite unambiguous. Although there was significant loss of IHCs and OHCs in the extreme base in all but the neonatal case, there was

diffuse hair cell loss, especially among OHCs, throughout the cochlear spiral in all the adult ears. Counts of 4th row OHCs, added for completeness, tend to be higher in the apical half of the cochlea. The relatively low “survival” of cells in this row, *re* the other rows, is an artifact of the algorithm, i.e. dividing the number of OHCs observed in each row by the number expected in the 1st row. The 4th row is most irregular and would not be present at 100% even at birth.

The overall patterns of hair cell survival vs. cochlear frequency, or vs. age, are best seen in the mean data in Fig. 3. Although both IHC and OHC means (Fig. 3A, B, respectively) show the expected high-frequency loss, especially in the oldest ears, OHCs also show dramatic degeneration at the apical end. Given the well-known trends toward high-frequency hearing loss in aging ears (Gordon-Salant, 2005), it was surprising to see a relatively flat loss of OHCs across the audiometric range (0.25–8.0 kHz; Fig. 3B). The loss of hair cells with age was significant in all cochlear regions: e.g. $r^2 = 0.37$, $p = 0.004$ for IHCs and $r^2 = 0.417$, $p = 0.002$ for OHCs when averaged across all audiometric frequencies. As shown in Fig. 3C, D, the slopes of age-related IHC or OHC loss were not significantly different when comparing the low-frequency region (0.25–1.0 kHz) to the high-frequency (1.4–8.0 kHz) region of the audiometric range ($p = 0.33$ for IHCs and $p = 0.23$ for OHCs by a Z test). We compared the age-related loss of IHCs and OHCs for males vs. females in our sample (averaging over the entire audiometric range) and saw no significant effect of gender.

Patterns of type-I neuronal loss

The organ of Corti makes synaptic connections with two kinds of afferent fibers that carry sensory information to

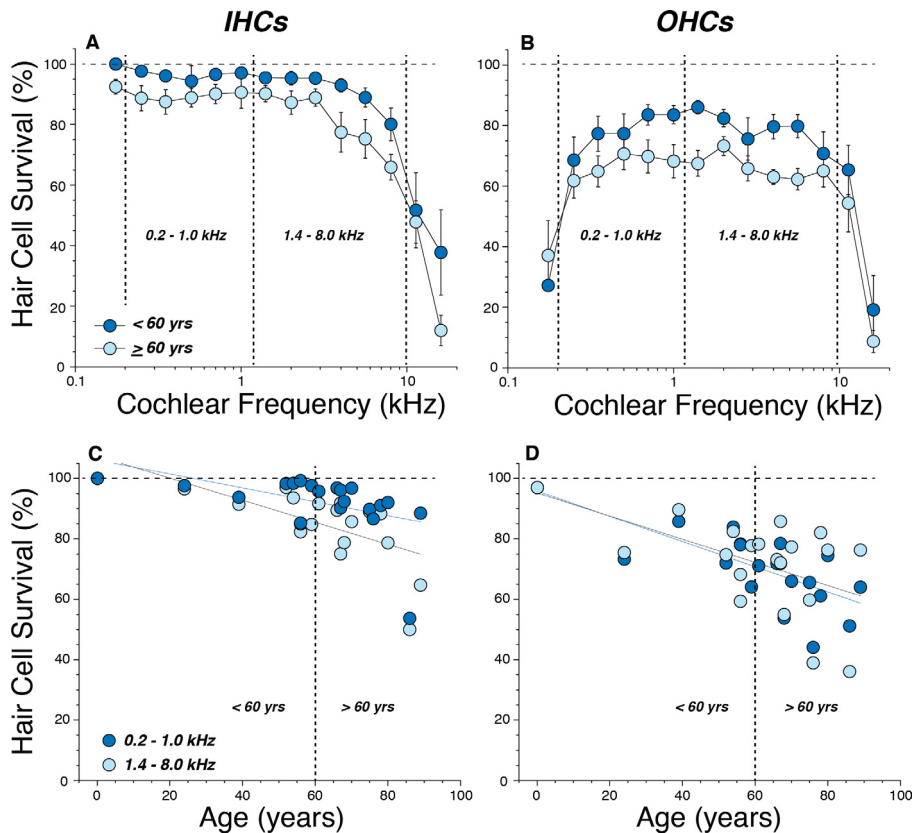


Fig. 3. Hair cell counts decrease with age throughout the cochlear spiral. (A, B) Mean survival (\pm SEM) of IHCs (A) and OHCs (B) as a function of cochlear location/frequency for all the wholemount ears in the present study, arbitrarily divided into those older or younger than 60 yrs. Vertical dashed lines show the frequency binning used in the lower panels to compare apical vs. basal cochlear regions within the audiometric range. (C, D) Mean survival of IHCs (C) and OHCs (D) as a function of age, with data from each ear averaged separately for apical and basal regions, as schematized in A and B. Best-fit straight lines for each subset is shown in each panel.

the brain, and two kinds of efferent neurons carrying feedback signals from the brain back to the periphery. Here, we are interested in the sensory fibers, including both (1) a majority (90%) population of myelinated “type I” ANFs innervating exclusively IHCs and (2) a minority (10%) unmyelinated population of “type II” ANFs, innervating exclusively OHCs (Nayagam et al., 2011). To quantify the survival of type-I’s, we immunostained with antibodies to neurofilament (green fluorophore in Fig. 4), a major component of all neurons in the inner ear. To distinguish type-I from type-II axons, we used a fluorescent membrane dye (Cellmask Orange®, the red fluorophore in Fig. 4, which brightly stains myelin sheaths. At the same cochlear location where we imaged hair cells, we obtained z-stacks through the osseous spiral lamina to image the ANF peripheral axons. As shown in Fig. 4, these z-stacks can be digitally re-sliced, to produce virtual cross-sections, in which myelinated fibers can be counted. These myelinated axons often appear varicose in longitudinal section, as shown at the white arrow in Fig. 4B. This is presumably a post-mortem artifact, as it is not observed in well-fixed animal material (data not shown). This artifact can explain why the Cellmask-positive elements in the virtual cross-sections are of such uneven diameter (see insets to Fig. 4A, B).

To identify olivocochlear efferent neurons, we used an antibody to a cholinergic marker, choline acetyltransferase (ChAT, blue fluorophore in Fig. 4. Consistent with the known anatomy (Liberman and Brown, 1986), these efferent bundles take a spiral course through the osseous spiral lamina (blue filled arrows in Fig. 4A), before turning radially to travel toward the sensory epithelium. The ChAT immunolabel allows us to differentiate efferent from afferent fibers, e.g. the blue-filled arrow in the inset to Fig. 4A. Although animal work shows that efferents projecting to the OHC region are typically myelinated outside of the sensory epithelium, in the present study, we rarely observed myelinated ChAT-positive fibers in the osseous spiral lamina. Thus, the ChAT label is not necessary for human counts of type-I afferents, at least in the osseous spiral lamina.

As in other mammalian species (Liberman, 2017), the density of type-I ANFs in our human ears peaks in the middle of the cochlea (Fig. 5A), with more than $5\times$ times as many fibers per unit length of organ of Corti near the 1-kHz region as in the apical and basal extremes of the spiral. Arbitrarily separating our population into those older or younger than 60 yrs suggests an

effect of age, which is considered more explicitly below. Counting IHCs in the same z-stacks allows us to express the ANF density as fibers per surviving IHC, as shown in Fig. 5B. The results suggest that the rate of neuronal loss exceeds the rate of IHC loss (see Discussion). The striking increase in ANFs/IHC at the extreme cochlear base suggests that the peripheral axons degenerate much more slowly than the IHCs in this region. To more accurately compare the rates of ANF and IHC loss, it is useful to express the neuronal survival in the same way as IHC survival is expressed, i.e. with respect to the normal number of IHCs per mm of cochlear length, which varies as a function of cochlear location (Fig. 5C). This transformation is applied in Fig. 5D.

These transformed values, averaged separately for low- and high-frequency regions of the audiometric range (Fig. 6), show a strong correlation between ANF survival and age in both halves of the cochlea: $r^2 = 0.69$ for the low-frequency region ($p < 0.0001$, Fig. 6A) and $r^2 = 0.81$ for the high-frequency region ($p < 0.0001$, Fig. 6B). Because our sample of cochlear wholemounts includes only three subjects under the age of 40, we supplemented the analysis with two 7-year-old ears from a prior study of osmium-stained cochlear

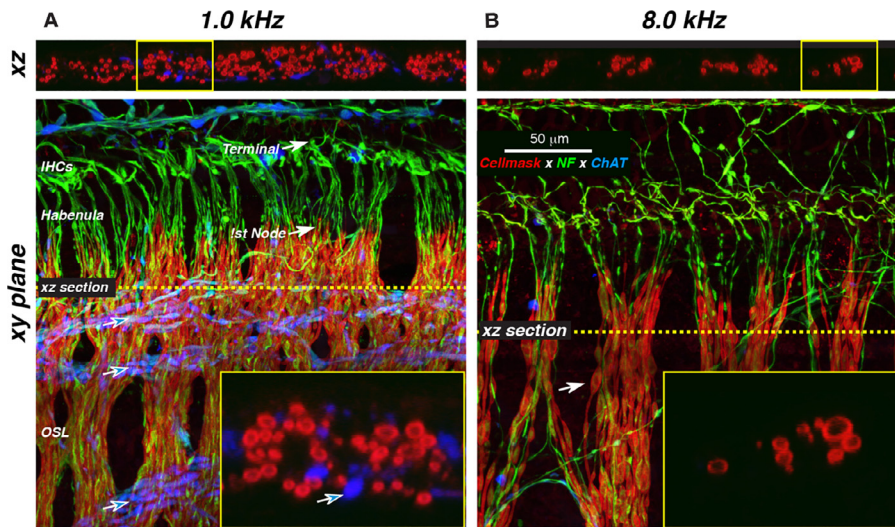


Fig. 4. Confocal projections from wholemounds of the osseous spiral lamina showing the type of virtual cross-sections used to count ANF peripheral axons. (A, B) Images from the 1.0- and 8.0-kHz regions, respectively of a 78-year-old male. The large, lower image in each panel shows the maximum projection of the z-stack in the acquisition plane (xy). The smaller upper image shows an xz (cross)-section at the y location indicated by the dashed yellow line: the green (anti-neurofilament) channel has been suppressed for the sake of clarity. The yellow box in each xz slice delineates the region shown at higher magnification at the bottom right. The blue-filled arrows in A point to the spiraling bundles of efferent (ChAT-positive) fibers. The white-filled arrows in A delineate the unmyelinated portion of ANFs, i.e. the region between the IHC-contacting terminal and the first node of Ranvier. The white-filled arrow in B points to a varicosity in a single ANF peripheral axon. Color key and scale bar in B applies to both panels. Hair cells were imaged on a 4th channel in each z-stack, but are not displayed here for the sake of clarity.

wholemounts (stars in Fig. 6, (Spendlin and Schrott, 1990), and 7 ears ranging in age from a few days to 24 yrs from our collection of archival serially sectioned temporal bones here at the MEEI (squares in Fig. 6. The slope of the resultant relation between ANF survival and age was steeper in the high-frequency region (-0.123 fibers/IHC/yr) than in the low-frequency region (-0.0843 fibers/IHC/yr), and the difference was statistically significant ($p = 0.01$ by a Z test). We compared the age-related loss of ANFs for males vs. females in our sample (averaging over the entire audiometric range) and saw no significant effect of gender in this small sample.

Patterns of type-II neuronal loss

The type-II fibers are thin and unmyelinated throughout their entire course from OHCs to the cochlear nucleus, and their functional role in hearing is poorly understood, though longstanding speculation (Simmons and Liberman, 1988) and recent empirical evidence (Flores et al., 2015; Liu et al., 2015) suggest they may be involved in nociception. In contrast to type-I fibers, each of which typically innervates a single IHC by a single synaptic contact, each type-II fiber spirals beneath the OHCs sending off multiple branchlets to contact multiple (up to 100) OHCs, usually within a single row (Simmons and Liberman, 1988). These outer spiral fibers, as they are called, stain well with anti-neurofilament antibody, thus, the bundles they form under the OHCs are easily seen in confocal projections (Fig. 7). The images in Fig. 7 sug-

gest that the number of outer spiral fibers is higher in apical cochlear regions than in the base.

Because of their small caliber, it was not possible to count these unmyelinated axons in either the osseous spiral lamina or the organ of Corti. Instead, we estimated outer spiral fiber density by measuring their silhouette area in maximal projections of the OHC region, such as those in Fig. 7. As summarized in Fig. 8A, the mean data suggest that the type-II innervation of OHCs is maximal around the 0.3 kHz region and declines monotonically from there to the apical and especially the basal extremes. Although the arbitrary separation of our cases into those older or younger than 60 yrs (Fig. 6A) suggests an age-related decline in type-II innervation density, an assessment of the regression of density vs. age shows no significant trends in either apical or basal cochlear regions: $r^2 = 0.06$, $p = 0.32$ in the apex; $r^2 = 0.01$, $p = 0.66$ in the base). This stands in stark contrast to the clear age-related declines in the density of type-I fiber innervation shown in Fig. 6.

DISCUSSION

Age-related degeneration of inner and outer hair cells

There is a large epidemiological literature showing that audiometric thresholds deteriorate faster with age at high frequencies than at low frequencies (Gordon-Salant, 2005). For example, men in their 9th decade show a 40 dB difference in threshold shifts at 0.25 kHz (30 dB) vs. 8.0 kHz (70 dB) (Gordon-Salant, 2005). In contrast, it is difficult to find a quantitative overview of the age-related changes in hair cell survival in the human ear. There are several reasons for this. Firstly, human temporal bone histopathology is typically presented as case studies (McGill and Schuknecht, 1976; Nadol, 1990; Felix et al., 1990; Felder and Schrott-Fischer, 1995; Hinojosa et al., 2001; Chen et al., 2006), and hair cell survival data are rarely averaged across cases. Secondly, many histopathological studies of human presbycusis are carried out on sectioned material, using an analysis protocol whereby hair cells are rated as either present or absent (McGill and Schuknecht, 1976; Nadol, 1990; Schuknecht, 1993; Hinojosa et al., 2001; Chen et al., 2006). Using such a binary rating scheme, all the cytochleograms in Fig. 2 would look similar and would only show hair cell loss in the extreme basal cochlear region.

Here, with immunostained cochlear wholemounds, the normally regular cellular array allows accurate estimates

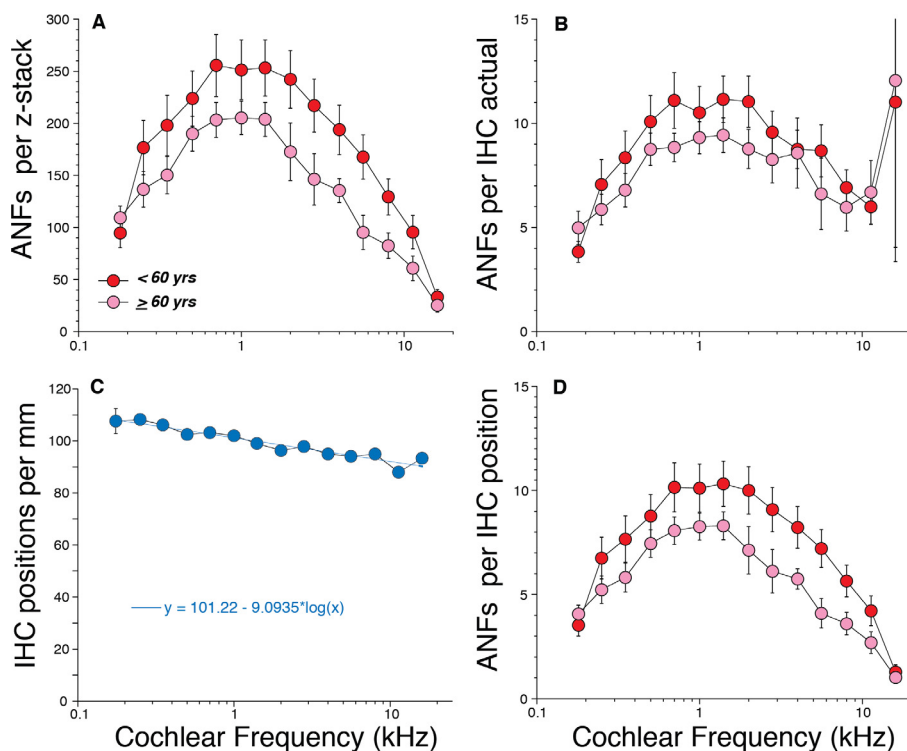


Fig. 5. ANF peripheral axon counts peak in the middle of the cochlea and decline with age. (A) ANF counts vs. cochlear frequency/location for all wholemount ears in the present study, arbitrarily divided into those older or younger than 60 yrs. Data are extracted from digital cross-sections of confocal z-stacks like those in Fig. 4, and are expressed as axons per z-stack, each of which spans 246 μm of cochlear length. (B) The same data as in A, except that the counts per z-stack are divided by the number of surviving IHCs counted in the same stack. (C) The normal density of IHC positions/mm as a function of cochlear location, i.e. the number of IHCs originally present, as extrapolated from regions with minimal loss, e.g. Fig. 1A. A best-fit straight line is shown ($r^2 = 0.91$), along with the equation that describes it. (D) The same data as in A, except that the counts per z-stack have been divided by the normal density of IHCs in the appropriate cochlear region (from C). All data are means (\pm SEM). Symbol key in A applies to all panels.

surprising, given the general view that presbycusis involves an apically progressing wave of hair cell death beginning at the high-frequency (basal) end (Schuknecht, 1993). What is more surprising is the loss of OHCs in the apical extreme. Although this pattern can be seen in some prior human case studies (Felix et al., 1990), the overall prevalence was not obvious from prior human work, though an apical focus of hair cell loss is seen in aging mice (Sergeyenko et al., 2013). What is most surprising is the relative constancy OHC loss across all the audiometric frequencies (0.25–8.0 kHz: Fig. 3B, D). Given the overwhelming evidence for high-frequency hearing loss in the aging ear (Gordon-Salant, 2005), and the notion that OHC survival should be a major determinant of age-related threshold shift, an apical to basal gradient in OHC loss would be expected. There are several ways to think about this apparent discrepancy. First, the OHC “motors” may contribute less to cochlear amplification in the cochlear apex than at the cochlear base (Liberman et al., 2002). Thus, the same amount of OHC loss at the apex might cause less threshold shift than at the base. It is also possible that the basal IHC loss contributes to the threshold shift, although such a suggestion contradicts evidence that scattered IHC loss has little effect on thresholds until it exceeds 80% (Lobarinas et al., 2013). Lastly, damage to other structures not evaluated here, e.g. hair cell stereocilia (Liberman and Dodds, 1984) or the stria vascularis (Pauler et al., 1988) could represent additional functionally important structural changes.

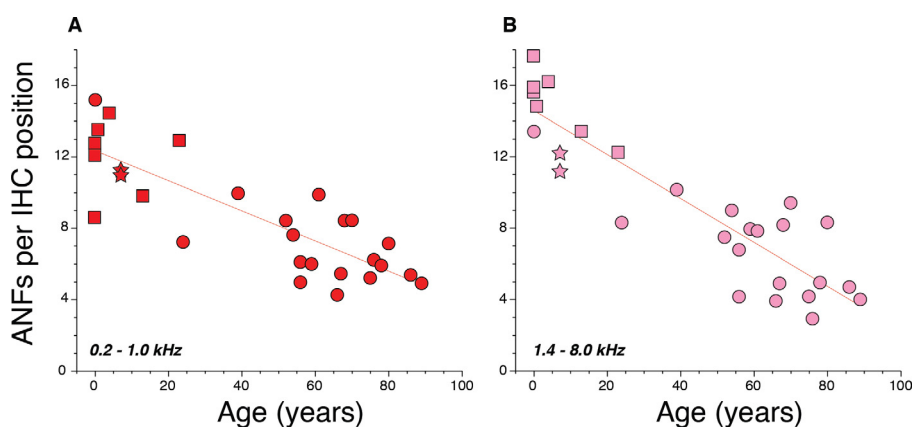


Fig. 6. The age-related decline in peripheral axon counts is steeper in the basal half of the cochlea (B) than in the apical half (A). (A, B) Mean number of ANFs in each case, as averaged over the cochlear frequency range indicated. Data are expressed as fibers/mm divided by the normal number of IHCs/mm at that location (see Fig. 5D). Data from wholemounts are shown by filled circles; data from archival sections by filled squares and data from a prior study (Spoendlin and Schrott, 1990) as filled stars. Best-fit straight line to each scatterplot is shown: $y = -0.0843x + 12.36$, $r^2 = 0.69$ in A; $y = -0.123x + 14.594$, $r^2 = 0.81$ in B.

Type I vs. Type II innervation density and age-related degeneration

As in all mammals examined, the density of synapses/IHC in humans shows a peak in the middle of the cochlea, with lower densities toward the base and apex Fig. 5. Since each type-I

of fractional survival. The mean cytochleograms in Fig. 3 are interesting in several respects. The death of both IHCs and OHCs at the high-frequency end is not

ANF typically contacts a single IHC by a single synapse (Liberman, 1980), these synaptic counts also reflect the

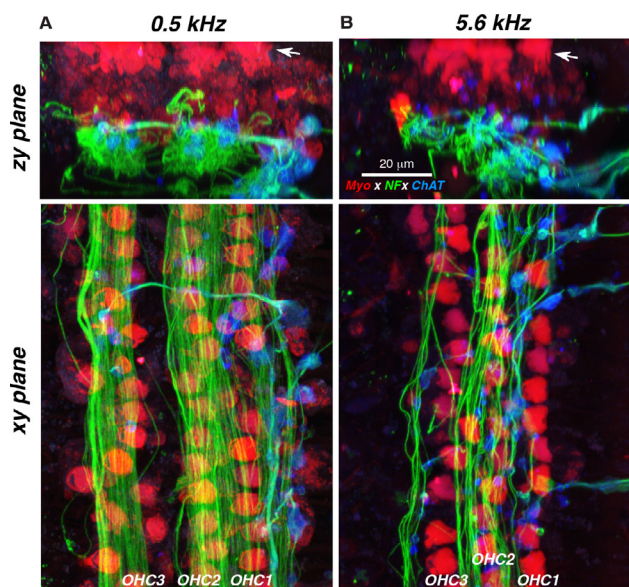


Fig. 7. Confocal projections from wholemounts of the organ of Corti showing the OHC region in two cochlear locations from a 39-year-old female. (A, B) In each column, one cochlear region is shown as a maximum projection in the acquisition plane (*xy*) and in the *yz* plane, i.e. a digital cross-section through the epithelium. The 1st-row OHCs (OHC1) are closest to the IHCs. The white arrows in A and B point to the brightly stained cuticular plates of the hair cells. Scale bar and staining key in B applies to all panels.

density of type-I ANFs per IHC. Curiously, the peak innervation density in humans (~ 16 ANFs per IHC in the youngest ears – Fig. 6 is among the lowest reported, compared, for example, to 18 in mouse (Liberman et al., 2015), 18 in chinchilla (Hickox et al., 2017), 18 in rhesus (Valero et al., 2017), 20 in guinea pig (Furman et al., 2013), 24 in rat (Hickox et al., 2017), and 30 in cat (Liberman et al., 1990). However, the number of ANFs per octave along the cochlear spiral is likely larger in humans, because the human cochlea is longer (32–35

mm), while the number of octaves spanned (6–7) and the density of IHCs/mm (~ 100) is similar across mammalian species.

The normal distribution of type-II neurons along the cochlear spiral has been less extensively studied. Type-II ganglion cell counts in rat show an apex-to-base distribution similar to that seen here Fig. 8 for peripheral terminals, i.e. strongly peaking in the upper middle turn and falling off more apically and basally (Keithley and Feldman, 1979). Such a differential distribution of cell bodies would be amplified in the distribution of peripheral terminals (as assessed here), because each apical type II spirals for longer distances and innervates more OHCs than each type II in the base (Simmons and Liberman, 1988). Recent work in mouse suggests that type II's comprise two chemically distinct neuronal populations with opposing gradients (Sherry Wu et al., 2018): an apically distributed group is positive for tyrosine hydroxylase, suggesting an analogy to pain-sensing C fibers in the somatosensory system, while a basally distributed group expresses the peptidergic transmitter CGRP, suggesting an analogy to low-threshold mechanoreceptive C fibers. The idea that the unmyelinated type II neurons are involved in pain or auditory nociception is a longstanding one (Simmons and Liberman, 1988), for which there is now more direct empirical evidence (Flores et al., 2015; Liu et al., 2015).

In the present study, type-II terminals in the OHC region did not show a significant age-related decline Fig. 8, despite a significant loss of OHCs, suggesting an overall increase in the ratio of type II to type I innervation in the aging ear. Such a trend is intriguing in light of the idea that type II's are involved in pain sensation and the observation that hyperacusis, i.e. intense auditory discomfort associated with moderate-level sounds, also increases in the aging ear (Tyler et al., 2014).

Prior literature has suggested that, as seen here, type-II's are more resistant to degeneration than type I's. For example, if ANF central axons are severed, near the Schwann-Glial border, there is a rapid (within days), massive degeneration of type-I neurons, while type-II neurons survive in large numbers for many months (Spoendlin, 1971). This originally suggested that type II's do not project to the brainstem, but that is not the case (Ryugo et al., 1991), and the reason(s) for the differential survival remain unclear. A prior study suggested that type II's double from 5% to 10% of the surviving ganglion-cell population in the aging rat, although both neuronal types clearly decrease in absolute numbers (Keithley and Feldman, 1979). In contrast, a prior human aging study concluded that the ratio of type II to type I cell bodies does

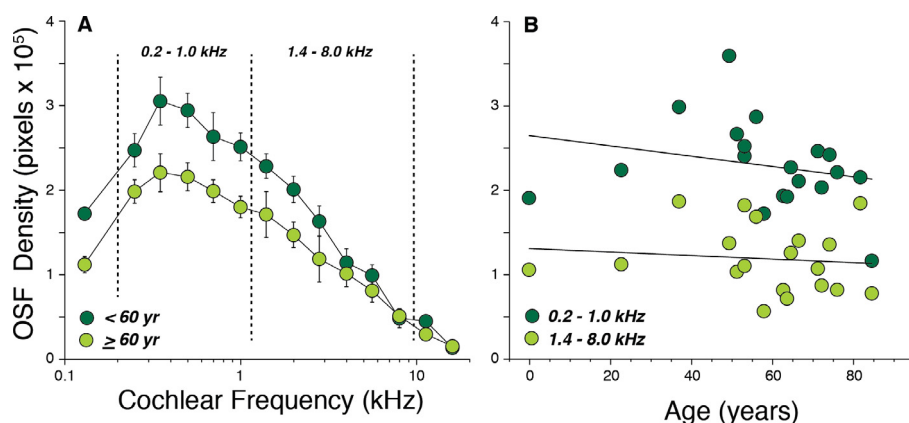


Fig. 8. The density of outer spiral fibers (OSFs) peaks closer to the cochlear apex, and does not decline with age as steeply, as myelinated ANFs. (A) Mean OSF density (\pm SEM) for all the wholemount ears in the present study, arbitrarily divided into those older or younger than 60 yrs of age. (B) Mean density of OSFs in each case, as averaged over the cochlear frequency range indicated. The best-fit straight line for each scatterplot is shown: $r^2 = 0.01$ (base), $r^2 = 0.06$ (apex). The OSF densities were extracted from the green channel of maximum projections such as those in Fig. 7 and are expressed as the mean number of suprathreshold pixels per image.

not change, despite considerable decline in total neural counts (Zimmermann et al., 1995), however that study included ears with widespread loss of all cochlear sensory cells, which was not the case here.

Type-I degeneration and inner hair cell loss

The degenerative behavior of type-I ANFs is complex and is influenced by a host of factors including (1) the nature, severity and locus of the insult, and (2) the patterns of damage/survival among the other cells that they contact in the inner ear. In cochlear insults such as noise damage and ototoxic drugs, the death of type-I SGCs and their central axons is slower, and less complete, than the loss of IHCs (Liberman and Kiang, 1978; Hinojosa et al., 2001). This observation led to the dogma that, in acquired SNHL, IHC death is the primary event, while neuronal loss is secondary to the loss of peripheral contacts. For example, after noise damage in cat IHC loss appears within days, while loss of peripheral axons appears only after a few weeks, and loss of SGCs only after a few months (Liberman and Kiang, 1978). Similarly, after aminoglycoside ototoxicity in guinea pigs, IHC loss in the basal turn exceeds 70% at 1 wk and 90% at 4 wks post treatment, while SGC loss was <25% at 1 wk and <60% at 4 wks (Kong et al., 2010). Other studies confirm the idea that SGC loss asymptotes at ~60% by ~6 wks post aminoglycoside deafening (van Loon et al., 2013). However, there may also be a slower wave of SGC death: aminoglycoside-deafened cats show continued SGC loss from ~60% at 1 year to >95% at 3 yrs post treatment (Leake and Hradek, 1988).

In human studies, SGC degeneration appears even slower *re* the rate of hair cell loss. One study of a human given gentamycin and tobramycin at high enough doses to destroy all IHCs in the basal third of the cochlea showed no significant loss of SGCs at the time of death 8 wks later (Hinojosa et al., 2001). This slower degenerative time course could be due to dosing difference rather than species difference: the human case received 2 mg/kg/day (Hinojosa et al., 2001), whereas a typical guinea pig study uses 400 mg/kg/day, in combination with furosemide to increase entry into the cochlea (van Loon et al., 2013). Another human study of idiopathic SNHL describes four cases with complete loss of IHCs throughout the basal half of the cochlea associated with only 10–50% loss of SGCs, despite hearing-loss durations of 11–29 yrs (Linthicum and Fayad, 2009). In all these cases, the loss of ANF peripheral axons appears nearly complete in regions of IHC loss. Thus, many SGCs apparently survive with only central axons intact. These disconnected neurons must generally remain functional, given the success of cochlear implants in profound deafness of longstanding duration.

Although the degree and time course of cell death may differ in IHC vs. SGC populations, the spatial patterns of cell death in the two cell types are often similar, further suggesting that SGCs degenerate as a direct result of the death of IHCs. However, recent mouse studies, in which genetic manipulations can be used to selectively kill IHCs without delivery of noxious sound or toxic chemicals to the ear, show that IHC

death need not lead to SGC degeneration (Zilberstein et al., 2012; Tong et al., 2015), at least for survival times as long as 3 months. Several lines of evidence suggest that IHC supporting cells, and the neurotrophin signaling pathways they subserve, are most important to neural survival in the adult ear (Stankovic et al., 2004; Wan et al., 2014). Conversely, if SGCs are directly destroyed, as after sectioning their central axons, there can be minimal loss of IHCs, even years after surgery (Sugawara et al., 2005). Thus, the survival of neither hair cells nor ganglion cells appears to require the survival of the other synaptic partner, and whatever tendency there is for spatial overlap of their degeneration likely arises because the relevant insult directly affected both cell types in similar regions.

Type-I degeneration and hidden hearing loss

The present study was inspired by animal work showing that massive ANF degeneration can occur without IHC death after noise exposure (Kujawa and Liberman, 2009) and before IHC death in aging (Stamatakis et al., 2006; Sergeev et al., 2013). Here we show, among “normal-aging” people without any explicit audiological or otologic complaints, a progressive, age-related deafferentation of surviving IHCs similar to that seen in mouse. Prior animal work on primary ANF degeneration analyzed the peripheral terminals of ANFs and their synapses with IHCs, because they are easily quantified, and because they appear to be the first elements to disappear after noise (Liberman et al., 2015). Here, we counted peripheral axons. Although synaptic puncta are visible in IHCs from human temporal bones (Viana et al., 2015), and in the wholemount specimens studied here, the IHC region is particularly vulnerable to post-mortem autolysis, whereas myelinated nerve fibers are not (Nadol and Burgess, 1985). An early post-mortem change is swelling of nerve terminals under the IHCs and lysis of the IHC basolateral membrane. Such lysis might result in dispersion of the synaptic puncta and reduction in synaptic counts in post-mortem material. Although myelinated axons become varicose in post-mortem material, there is no evidence that they lyse: i.e. individual axons can virtually always be followed from proximal to distal locations within the osseous spiral lamina in our confocal z-stacks. Thus, the fluorescent membrane stain we use here (CellMask) is likely to provide the best estimate of the intact afferent innervation pre-mortem.

There are several prior studies of primary neural degeneration, i.e. ANF loss without commensurate IHC loss, in the human literature. A study of three ears age 53–67 yrs with high-tone hearing loss and poor speech discrimination scores (70–75% in quiet) vs. two “controls” (similar ages, but with 100% speech scores), used plastic-embedded, osmium-stained wholemounts to count hair cells and then sectioned the plastic blocks to count ANF peripheral axons (Felder and Schrott-Fischer, 1995), much as we did here using virtual resectioning of confocal z-stacks. Despite minimal IHC loss, there was 30–40% loss of peripheral axons in the poor-performing ears. Another, more recent study of serially sectioned human temporal bones suggests that a special

subset people older than 65 have “neuritic presbycusis”, defined as a significant loss of ANF peripheral axons despite “normal” ganglion-cell and hair-cell populations. However, the cruder nature of hair cell counts in this type of histological material, and a cruder estimate of neuronal survival, make these data somewhat less compelling (Chen et al., 2006).

Here, our data suggest that age-related loss of ANF peripheral axons outstrips the rate of age-related IHC loss by a factor of 2.6: i.e. 7.7% loss of ANFs per decade vs 2.9% loss of IHCs per decade (Fig. 9), when averaging across cochlear regions corresponding to all the audiometric frequencies. The difference in slopes of these two regressions was highly significant ($p < 0.0001$ by a Z test). The rate of peripheral axon loss also outstrips the rate of SGC loss (black symbols in Fig. 9, derived from a prior temporal bone study of archival cases with minimal IHC loss and without explicit audiological or otologic complaints (Makary et al., 2011). This suggests that many SGCs survive in aging ears without peripheral axons, thus disconnected from the surviving IHCs they once contacted. It may be significant that the young adult case with exposure to cisplatin, a known ototoxin (arrow in Fig. 9, shows a relatively low peripheral axon count compared with the minimal loss of IHCs. As with noise damage, cisplatin may cause cochlear neuropathy before it destroys hair cells.

Here, a number of subjects over 50 yrs showed deafferentation exceeding 60%, even when averaged over

all the audiometric frequencies (Fig. 9). Behavioral studies in animals suggest that this degree of deafferentation would not affect the threshold audiogram (Schuknecht and Woellner, 1955; Lobarinas et al., 2013). However, it seems highly likely that this loss of information channels this represents would degrade signal-extraction in central pathways, especially in noisy listening environments (Lobarinas et al., 2016). Thus, it seems likely that the individuals with the worst deafferentation of IHCs would show signs of “hidden hearing loss”. It has also been suggested that this type of deafferentation might be a key elicitor of tinnitus via secondary changes in central gain” (Chambers et al., 2016).

Several lines of evidence suggest that this type of deafferentation could be reversed, even in adult ears, so long as the SGCs and IHCs survive. Years ago, several laboratories showed that, after ototoxin-induced destruction of the organ of Corti, cochlear perfusion of neurotrophins, key signaling molecules in normal neural development and survival, could promote SGC survival and neurite extension along the denuded basilar membrane, despite the lack of hair cell targets (Altschuler et al., 1999; Wise et al., 2005). More recently, our group showed that neurotrophin application to the round window 24 h after noise-induced cochlear deafferentation could restore synapses to surviving IHCs and rescue the associated functional deficits (Suzuki et al., 2016). Thus, if similar neurotrophin treatments can be successful at longer trauma-treatment intervals, such a therapeutic intervention could be meaningful in aging ears. The present data suggest that virtually everyone over 60 might show a clinically relevant improvement.

ACKNOWLEDGMENTS

The assistance of Diane Jones in temporal-bone removal and Dr. Felipe Santos in temporal-bone drilling of some cases is gratefully acknowledged. Research supported by the Lauer Tinnitus Center and by a program grant from the NIDCD (P50 015857).

REFERENCES

- Bohne BA, Harding GW (2000) Degeneration in the cochlea after noise damage: primary versus secondary events. *Am J Otol* 21:505–509.
- Liberman MC, Kiang NY (1978) Acoustic trauma in cats cochlear pathology and auditory-nerve activity. *Acta Otolaryngol* 358:1–63.
- Furman AC, Kujawa SG, Liberman MC (2013) Noise-induced cochlear neuropathy is selective for fibers with low spontaneous rates. *J Neurophysiol* 110:577–586.
- Kujawa SG, Liberman MC (2009) Adding insult to injury: cochlear nerve degeneration after “temporary” noise-induced hearing loss. *J Neurosci* 29:14077–14085.
- Johnsson LG (1974) Sequence of degeneration of Corti’s organ and its first-order neurons. *Ann Otol Rhinol Laryngol* 83:294–303.
- Johnsson LG, Hawkins Jr JE (1976) Degeneration patterns in human ears exposed to noise. *Ann Otol Rhinol Laryngol* 85:725–739.
- Sergeyenko Y, Lall K, Liberman MC, Kujawa SG (2013) Age-related cochlear synaptopathy: an early-onset contributor to auditory functional decline. *J Neurosci* 33:13686–13694.
- Stamatakis S, Francis HW, Lehar M, May BJ, Ryugo DK (2006) Synaptic alterations at inner hair cells precede spiral ganglion cell loss in aging C57BL/6J mice. *Hear Res* 221:104–118.

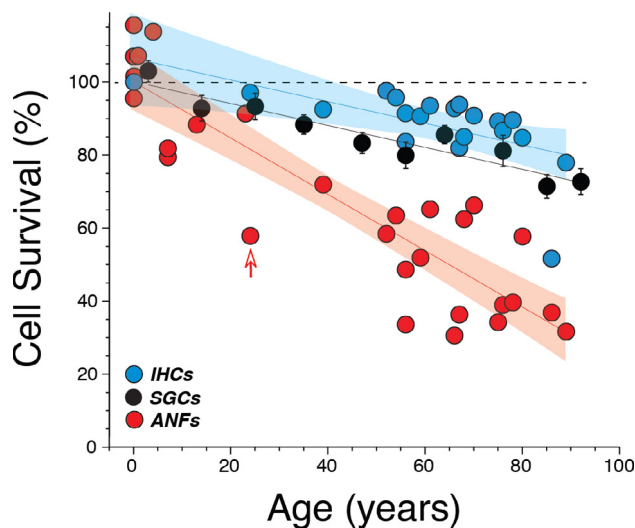


Fig. 9. The age-related loss of ANF peripheral axons is steeper than that for SGCs or IHCs. For ANF and IHC data, each point is the cell-survival in each case averaged over all sample points within the audiometric frequencies (0.25–8.0 kHz inclusive). The SGC data are from a prior study of normal aging individuals ($n = 10$ per decade of life (Makary et al., 2011), normalized to % survival using the y-intercept of the best-fit straight line. The ANF data are the same cases as in Fig. 6, but averaged over all points from 0.25 to 8.0 kHz, and also normalized using the best-fit straight line. Red arrow points to the one case exposed to a known ototoxin (cisplatin: see Table 1. IHC data are the same as in Fig. 2C, except averaged over all points from 0.25 to 8.0 kHz. IHC data were obtained as % survival and do not require normalization. The 95% confidence limits are shown for the IHC and ANF regressions.

- Woellner RC, Schuknecht HF (1955) Hearing loss from lesions of the cochlear nerve: an experimental and clinical study. *Trans Am Acad Ophthalmol Otolaryngol* 59:147–149.
- Lobarinas E, Salvi R, Ding D (2013) Insensitivity of the audiogram to carboplatin induced inner hair cell loss in chinchillas. *Hearing Res*. <https://doi.org/10.1016/j.heares.2013.03.012>.
- Zilberstein Y, Liberman MC, Corfas G (2012) Inner hair cells are not required for survival of spiral ganglion neurons in the adult cochlea. *J Neurosci* 32:405–410.
- Tong L, Strong MK, Kaur T, Juiz JM, Oesterle EC, Hume C, Warchol ME, Palmeter RD, Rubel EW (2015) Selective deletion of cochlear hair cells causes rapid age-dependent changes in spiral ganglion and cochlear nucleus neurons. *J Neurosci* 35:7878–7891.
- Badri R, Siegel JH, Wright BA (2011) Auditory filter shapes and high-frequency hearing in adults who have impaired speech in noise performance despite clinically normal audiograms. *J Acoust Soc Am* 129:852–863.
- Vermiglio AJ, Soli SD, Freed DJ, Fisher LM (2012) The relationship between high-frequency pure-tone hearing loss, hearing in noise test (HINT) thresholds, and the articulation index. *J Am Acad Audiol* 23:779–788.
- Liberman MC, Epstein MJ, Cleveland SS, Wang H, Maison SF (2016) Toward a differential diagnosis of hidden hearing loss in humans. *PLoS One* 11 e0162726.
- Spoendlin H, Schrott A (1990) Quantitative evaluation of the human cochlear nerve. *Acta Otolaryngol* 470:61–69 [discussion 69–70].
- Schuknecht HF (1993) *Pathology of the ear*. 2nd ed. Baltimore: Lea & Febiger.
- Greenwood DD (1990) A cochlear frequency-position function for several species—29 years later. *J Acoust Soc Am* 87:2592–2605.
- Liberman MC (1980) Morphological differences among radial afferent fibers in the cat cochlea: an electron-microscopic study of serial sections. *Hear Res* 3:45–63.
- O'Malley JT, Burgess BJ, Jones DD, Adams JC, Merchant SN (2009) Techniques of celloidin removal from temporal bone sections. *Ann Otol Rhinol Laryngol* 118:435–441.
- Gordon-Salant S (2005) Hearing loss and aging: new research findings and clinical implications. *J Rehabil Res Dev* 42:9–24.
- Nayagam BA, Muniak MA, Ryugo DK (2011) The spiral ganglion: connecting the peripheral and central auditory systems. *Hear Res* 278:2–20.
- Liberman MC, Brown MC (1986) Physiology and anatomy of single olivocochlear neurons in the cat. *Hear Res* 24:17–36.
- Liberman MC (2017) Noise-induced and age-related hearing loss: new perspectives and potential therapies. *F1000Res* 6:927.
- Simmons DD, Liberman MC (1988) Afferent innervation of outer hair cells in adult cats: I. Light microscopic analysis of fibers labeled with horseradish peroxidase. *J Comp Neurol* 270:132–144.
- Flores EN, Duggan A, Madathy T, Hogan AK, Marquez FG, Kumar G, Seal RP, Edwards RH, Liberman MC, Garcia-Anoveros J (2015) A non-canonical pathway from cochlea to brain signals tissue-damaging noise. *Curr Biol* 25:606–612.
- Liu C, Glowatzki E, Fuchs PA (2015) Unmyelinated type II afferent neurons report cochlear damage. *Proc Natl Acad Sci U S A* 112:14723–14727.
- McGill TJ, Schuknecht HF (1976) Human cochlear changes in noise induced hearing loss. *Laryngoscope* 86:1293–1302.
- Felder E, Schrott-Fischer A (1995) Quantitative evaluation of myelinated nerve fibres and hair cells in cochleae of humans with age-related high-tone hearing loss. *Hear Res* 91:19–32.
- Chen MA, Webster P, Yang E, Linthicum Jr FH (2006) Presbycusis neuritic degeneration within the osseous spiral lamina. *Otol Neurotol* 27:316–322.
- Felix H, Johnsson LG, Gleeson M, Pollak A (1990) Quantitative analysis of cochlear sensory cells and neuronal elements in man. *Acta Otolaryngol* 470:71–79.
- Hinojosa R, Nelson EG, Lerner SA, Redleaf MI, Schramm DR (2001) Aminoglycoside ototoxicity: a human temporal bone study. *Laryngoscope* 111:1797–1805.
- Nadol Jr JB (1990) Degeneration of cochlear neurons as seen in the spiral ganglion of man. *Hear Res* 49:141–154.
- Liberman MC, Gao J, He DZ, Wu X, Jia S, Zuo J (2002) Prestin is required for electromotility of the outer hair cell and for the cochlear amplifier. *Nature* 419:300–304.
- Liberman MC, Dodds LW (1984) Single-neuron labeling and chronic cochlear pathology. III. Stereocilia damage and alterations of threshold tuning curves. *Hear Res* 16:55–74.
- Pauler M, Schuknecht HF, White JA (1988) Atrophy of the stria vascularis as a cause of sensorineural hearing loss. *Laryngoscope* 98:754–759.
- Liberman LD, Suzuki J, Liberman MC (2015) Dynamics of cochlear synaptopathy after acoustic overexposure. *J Assoc Res Otolaryngol* 16:205–219.
- Hickox AE, Larsen E, Heinz MG, Shinobu L, Whitton JP (2017) Translational issues in cochlear synaptopathy. *Hear Res* 349:164–171.
- Valero MD, Burton JA, Hauser SN, Hackett TA, Ramachandran R, Liberman MC (2017) Noise-induced cochlear synaptopathy in rhesus monkeys (*Macaca mulatta*). *Hear Res* 353:213–223.
- Liberman MC, Dodds LW, Pierce S (1990) Afferent and efferent innervation of the cat cochlea: quantitative analysis with light and electron microscopy. *J Comp Neurol* 301:443–460.
- Keithley EM, Feldman ML (1979) Spiral ganglion cell counts in an age-graded series of rat cochleas. *J Comp Neurol* 188:429–442.
- Sherry Wu J, Vyas P, Glowatzki E, Fuchs PA (2018) Opposing expression gradients of calcitonin-related polypeptide alpha (Calca/Cgrpalpha) and tyrosine hydroxylase (Th) in type II afferent neurons of the mouse cochlea. *J Comp Neurol* 526:1073.
- Tyler RS, Pienkowski M, Roncancio ER, Jun HJ, Brozoski T, Dauman N, Dauman N, Andersson G, Keiner AJ, Cacace AT, Martin N, Moore BC (2014) A review of hyperacusis and future directions: part I. Definitions and manifestations. *Am J Audiol* 23:402–419.
- Spoendlin H (1971) Degeneration behaviour of the cochlear nerve. *Arch Klin Exp Ohren Nasen Kehlkopfheilkd* 200:275–291.
- Ryugo DK, Dodds LW, Benson TE, Kiang NY (1991) Unmyelinated axons of the auditory nerve in cats. *J Comp Neurol* 308:209–223.
- Zimmermann CE, Burgess BJ, Nadol Jr JB (1995) Patterns of degeneration in the human cochlear nerve. *Hear Res* 90:192–201.
- Kong WJ, Yin ZD, Fan GR, Li D, Huang X (2010) Time sequence of auditory nerve and spiral ganglion cell degeneration following chronic kanamycin-induced deafness in the guinea pig. *Brain Res* 1331:28–38.
- van Loon MC, Ramekers D, Agterberg MJ, de Groot JC, Grolman W, Klis SF, Versnel H (2013) Spiral ganglion cell morphology in guinea pigs after deafening and neurotrophic treatment. *Hear Res* 298:17–26.
- Leake PA, Hradek GT (1988) Cochlear pathology of long term neomycin induced deafness in cats. *Hear Res* 33:11–33.
- Linthicum Jr FH, Fayad JN (2009) Spiral ganglion cell loss is unrelated to segmental cochlear sensory system degeneration in humans. *Otol Neurotol* 30:418–422.
- Stankovic K, Rio C, Xia A, Sugawara M, Adams JC, Liberman MC, Corfas G (2004) Survival of adult spiral ganglion neurons requires erbB receptor signaling in the inner ear. *J Neurosci* 24:8651–8661.
- Wan G, Gomez-Casati ME, Gigliello AR, Liberman MC, Corfas G (2014) Neurotrophin-3 regulates ribbon synapse density in the cochlea and induces synapse regeneration after acoustic trauma. *eLife* 3.
- Sugawara M, Corfas G, Liberman MC (2005) Influence of supporting cells on neuronal degeneration after hair cell loss. *J Assoc Res Otolaryngol* 6:136–147.
- Viana LM, O'Malley JT, Burgess BJ, Jones DD, Oliveira CA, Santos F, Merchant SN, Liberman LD, Liberman MC (2015) Cochlear neuropathy in human presbycusis: confocal analysis of hidden hearing loss in post-mortem tissue. *Hear Res* 327:78–88.
- Nadol Jr JB, Burgess B (1985) A study of postmortem autolysis in the human organ of Corti. *J Comp Neurol* 237:333–342.
- Makary CA, Shin J, Kujawa SG, Liberman MC, Merchant SN (2011) Age-related primary cochlear neuronal degeneration in human temporal bones. *J Assoc Res Otolaryngol* 12:711–717.

- Schuknecht HF, Woellner RC (1955) An experimental and clinical study of deafness from lesions of the cochlear nerve. *J Laryngol Otol* 69:75–97.
- Lobarinas E, Salvi R, Ding D (2016) Selective inner hair cell dysfunction in chinchillas impairs hearing-in-noise in the absence of outer hair cell loss. *J Assoc Res Otolaryngol* 17:89–101.
- Chambers AR, Resnik J, Yuan Y, Whitton JP, Edge AS, Liberman MC, Polley DB (2016) Central gain restores auditory processing following near-complete cochlear denervation. *Neuron* 89:867–879.
- Altschuler RA, Cho Y, Ylikoski J, Pirvola U, Magal E, Miller JM (1999) Rescue and regrowth of sensory nerves following deafferentation by neurotrophic factors. *Ann N Y Acad Sci* 884:305–311.
- Wise AK, Richardson R, Hardman J, Clark G, O'Leary S (2005) Resprouting and survival of guinea pig cochlear neurons in response to the administration of the neurotrophins brain-derived neurotrophic factor and neurotrophin-3. *J Comp Neurol* 487:147–165.
- Suzuki J, Corfas G, Liberman MC (2016) Round-window delivery of neurotrophin 3 regenerates cochlear synapses after acoustic overexposure. *Sci Rep* 6:24907.

(Received 2 July 2018, Accepted 30 July 2018)
(Available online 10 August 2018)